# Evaluation of NASA GEOS-ADAS modeled diurnal warming through comparisons to SEVIRI and AMSR2 SST observations

**C.L. Gentemann[1] and S. Akella[2]**

[1]Earth and Space Research, Seattle, WA.

[2]GMAO, NASA GSFC and SSAI Inc.

Corresponding author: Chelle Gentemann (cgentemann@esr.org)

**Key Points:**

- Modeled diurnal warming is compared to collocated satellite observed diurnal warming.
- Overall the modeled warming is similar to the satellite warming in magnitude, spatial distribution, and variability.
- Weaknesses in the modeled warming were directly related back to specific features in the formulation of the model.

**Abstract**

An analysis of the ocean skin Sea Surface Temperature (SST) has been included in the Goddard Earth Observing System (GEOS) - Atmospheric Data Assimilation System (ADAS), Version 5 (GEOS-ADAS). This analysis is based on the GEOS atmospheric general circulation model (AGCM) that simulates near-surface diurnal warming and cool skin effects. Analysis for the skin SST is performed along with the atmospheric state, including Advanced Very High Resolution Radiometer (AVHRR) satellite radiance observations as part of the data assimilation system. One month (September, 2015) of GEOS-ADAS SSTs were compared to collocated satellite Spinning Enhanced Visible and InfraRed Imager (SEVIRI) and Advanced Microwave Scanning Radiometer 2 (AMSR2) SSTs to examine how the GEOS-ADAS diurnal warming compares to the satellite measured warming. The spatial distribution of warming compares well to the satellite observed distributions. Specific diurnal events are analyzed to examine variability within a single day. The dependence of diurnal warming on wind speed, time of day, and daily average insolation is also examined. Overall the magnitude of GEOS-ADAS warming is similar to the warming inferred from satellite retrievals, but several weaknesses in the GEOS-AGCM simulated diurnal warming are identified and directly related back to specific features in the formulation of the diurnal warming model.

## 1 Introduction

In clear sky, calm wind conditions, solar heating creates a thermally stratified layer in the upper ocean [*Price et al.,* 1987]. It is not uncommon for this surface diurnal layer to warm by more than 3K and persist for hours [*Minnett,* 2003; *Yokoyama et al.,* 1995; *Donlon et al*., 2007] . Spatially coherent, very large diurnal events, between 5 – 7 K have been observed in multiple collocated independent satellite measurements [*Gentemann et al.,* 2008]. The vertical distribution of the diurnal warming and its surface expression are determined by the absorption of solar radiation at differing depths (influenced by the light absorptivity of the water), the vertical diffusion of heat, the vertical stratification in the upper ocean 'mixed' layer, and the rate of turbulent mixing within the mixed layer. During the day, the Sea Surface Temperature (SST) at the surface, which interacts with the atmosphere, is the sum of the foundation temperature (the upper ocean temperature below the diurnal layer), the diurnal warm layer, and cool skin layer [*Donlon et al.,* 2007].

Atmospheric General Circulation Models (AGCMs) calculate heat fluxes between the atmosphere and ocean using SST. The SST is typically a daily (or monthly) gap-free analysis of satellite and in situ SST observations representing a bulk or foundation SST. Coupled models, take SST from an Ocean General Circulation Model (OGCM), which models the ocean state using the hydrostatic primitive equations and usually do not resolve the near-surface thermal structure well enough to simulate diurnal warming. Some ocean data assimilation systems also rely on daily or weekly (averaged) retrievals of bulk SST [*Reynolds et al.,* 2002; *Reynolds et al.,* 2007] and atmospheric fluxes from an already existing atmospheric reanalysis (see for e.g., [*Carton and Giese,* 2008; *Vernieres et al.,* 2012]); which in-turn rely on daily/monthly SST data products, therefore manyt coupled models, atmospheric and oceanic data assimilation systems do

not resolve the SST diurnal cycle. Failure to account for a diurnal cycle in SSTs in these models can lead to systematic errors in determining global SST and the surface fluxes that drive atmospheric circulations. *Zeng and Dickinson* [1998] found that the use of daily or monthly SSTs, instead of diurnally varying SSTs, results in under-estimates of latent heat by up to 10 $Wm^{-2}$ and sensible heat by 2-3 $Wm^{-2}$ during the daytime. They found little impact on monthly mean fluxes, but emphasized that the accurate diurnal fluxes could have an impact on the diurnal variation of clouds and precipitation. *Dai and Trenberth* [2004] examined how inclusion of diurnal variability in air temperatures, surface pressure, upper-air winds, and precipitation affected the skill of the Community Climate Model (CCM2). They concluded that the simulated diurnal cycle of precipitation was too weak over the oceans and that improvements in parameterization of the diurnal cycle in SSTs should lead to considerable improvements in the simulation of precipitation.

Several one-dimensional physical (e.g. [*Fairall et al.,* 1996a; *Large et al.,* 1994; *Price et al.,* 1986; Kawai and Kawamura, 2000]) and empirical (e.g. [*Webster et al.*, 1996; *Clayson and Curry*, 1996; *Gentemann et al.,* 2003; *Gentemann et al.,* 2009) models have been developed to describe the diurnal warm layer. An excellent review of these models is given in *Kawai and Wada* [2007]. Several of these models have been extensively tested and compared to in situ measurements under light to moderate wind conditions [*Anderson et al.,* 1996; *Shinoda and Hendon,* 1998]. These models have not been utilized in the modeling community either because they are not energy conserving, require inputs that are not available, or are not formulated in an easily adaptable manner.

*Zeng and Beljaars* [2005], hereafter ZB05, developed a prognostic model of skin SSTs that includes both the cool skin effect and diurnal warming variability, that is easily implemented into AGCMs. This work was extended to include the impact of Langmuir circulations on diurnal warming by *Takaya et al.* [2010a], hereafter TBBJ10. The model calculates the cool skin and warm layer effects using surface fluxes (net longwave and shortwave radiation, sensible and latent heat fluxes), and mixing processes (molecular and turbulent). These models were validated against 3 months of moored buoy data in the Arabian Sea. The TBBJ10 scheme showed better agreement (a Root Mean Square Error (RMSE) of 0.28 K versus 1.04 K) with the buoys' 0.17 m SSTs than the ZB05 and improved spatial distribution of diurnal variability when compared against observations from the Advanced Microwave Scanning Radiometer - Earth Observing System (AMSR-E). Yet, the authors acknowledged some weaknesses in the TBBJ10 formulation. Results showed that the TBBJ10 scheme under-estimated diurnal amplitudes for calm, clear sky, and over-estimated diurnal amplitudes in moderate-to-high winds. This was attributed to the upper ocean vertical profile assumption embedded in the TBBJ10 model. Nevertheless, the TBBJ10 model is a significant step forward and has been integrated into European Center for Medium range Weather Forecasting (ECMWF; [*Takaya et al.,* 2010a; *Takaya et al.,* 2010b; *Zeng and Beljaars,* 2005]), the Met Office [*While et al.*, 2017], Naval Research Lab (NRL; [*McLay et al.,* 2012]), and NASA's Goddard Earth Observing System (GEOS)- Atmospheric Data Assimilation System (ADAS), Version 5 (GEOS-5) (henceforth referred to as GEOS-ADAS; [*Akella et al.,* 2017]). Recently the GEOS-ADAS has been

modified to resolve the diurnal cycle in the SST (details are given below). In this study we examine the accuracy of the TBBJ10 model in the GEOS-ADAS by comparing the diurnal warming with the Spinning Enhanced Visible and InfraRed Imager (SEVIRI) and Advanced Microwave Scanning Radiometer 2 (AMSR2) SST retrievals. To maintain an independent comparison, the configuration of GEOS-ADAS used in this work did not assimilate brightness temperature observations from AMSR2 and window channels (10 - 12 μ range) of SEVIRI.

## 2 Data

### 2.1 GEOS-ADAS SSTs

The GEOS-AGCM upper ocean temperature is calculated as $T(z) = T_d - \Delta T_c + \Delta T_{dw}(z)$ where $T_d$ is the foundation temperature from Operational Sea Surface Temperature and Sea Ice Analysis (OSTIA SST; *Donlon et al.* [2011]); $\Delta T_c$ and $\Delta T_{dw}$ respectively denote the cool skin and diurnal warm layer temperature changes and *z* denotes depth. $\Delta T_c$ and the depth of cool-skin layer ($\delta$) are based on *Fairall et al.* [1996b], calculation of $\Delta T_{dw}$ is explained shortly. Model temperature, atmospheric fields and observations are used by the GEOS atmospheric analysis to calculate analyzed fields of surface pressure (p), three-dimensional fields of virtual temperature ($T_v$), specific humidity ($q$), zonal and meridional winds ($u,v$) and also skin SST (i.e, $T(z \approx 0)$) [*Akella et al.,* 2017]. The difference between the analyzed and AGCM predicted fields (*u, v, p, $T_v$, q, skin SST*) are then utilized as increments in the next AGCM integration, following the Incremental Analysis Update (IAU) procedure [*Bloom et al.,* 1996]. Results presented in this paper are based on a cube sphere C360 (about 25km; [*Putman and Lin,* 2007]) grid resolution, with a three-dimensional variational analysis. All the atmospheric observations (satellite radiance plus in-situ) and Advanced Very High Resolution Radiometer (AVHRR) (channels 4 and 5 of NOAA-18 and Metop-A) available within the GEOS-ADAS have been used to analyze the atmospheric state, including the skin SST. For the present comparison, we have used hourly time averaged output at about 25 km.

The GEOS-AGCM diurnal warming is based on TBBJ10, with following three modifications. Due to absence of a wave model in GEOS, a global constant value of 1cm/s is used for the Stokes velocity to compute the Langmuir number (*Akella et al*., 2017), the procedure to simulate the slow decay of diurnal warming in the late afternoon described by ZB05 and also TBBJ10 was not included, and the shortwave absorption includes absorption in the visible and ultraviolet part of the spectrum based on the turbidity/biological activity. The diurnal warm layer depth, $d$ is set to 2.0 m and $\nu$, which sets the profile shape,

$$\Delta T_{dw}(z) = \left[1 - \left(\frac{z-\delta}{d-\delta}\right)^{\nu}\right] \Delta T_{dw}$$

of heating within the warm layer is set to 0.2 (~~please see~~ *Akella et al*., 2017 provide details on the choice of these parameter settings), and does not evolve while the model is integrated in time.

The core of the diurnal warming calculations in the GEOS-AGCM are based on TBBJ10, and are given below:

$$\frac{\partial \Delta T_{dw}}{\partial t} = \frac{(1+\nu)Q_w}{\nu d \rho_w c_w} - \frac{(1+\nu)\kappa u_{*w} f(La)}{d\phi_h(\zeta)} \Delta T_{dw} \quad [1]$$

$$\phi_h(\zeta) = \begin{cases} 1 + \dfrac{5\zeta + 4\zeta^2}{1 + 3\zeta + .25\zeta^2} & \text{if } \zeta > 0 \\ (1 - 16\zeta)^{-1/2} & \text{if } \zeta < 0 \end{cases} \quad [2]$$

$\phi_h(\zeta)$ , Equation 2, is the non-dimensional shear function or similarity model. $\rho_w$, $c_w$ , and $\alpha_w$ are the density, heat capacity, and thermal expansion coefficient of sea water, respectively. $Q_w$ is the net surface heat flux in the warm layer, and is determined from the sensible heat flux, latent heat flux, incoming shortwave absorption, and outgoing longwave emission, $\kappa$ is the von Karman constant (=0.4), $u_{*w}$ is the friction velocity of water, $f(La)$ is a function of the Langmuir number (La), and $\zeta = -z/L$ is the stability parameter with the Monin-Obukhov length defined as: :

$$L = \frac{\rho_w c_w u_{*w}^3}{\kappa g \alpha_w Q_w} \quad [3]$$

In *Akella et al.* [2017] the diurnal warming was evaluated by comparing to withheld drifting buoys. The calculated diurnal warming was close to the observations in the morning and afternoon, but in the late-afternoon to evening diurnal warming was found to be less than observed. In this paper we further test the GEOS-ADAS diurnal warming through comparisons to satellite data.

2.2 SEVIRI SSTs

Hourly 0.05 deg. gridded SEVIRI METEOSAT-10 Third Generation (MSG3) SSTs processed at the European Organization for the Exploitation of Meteorological Satellites (EUMETSAT) Ocean and Sea Ice Satellite Application Facility (OSI-SAF) into Group for High Resolution SST (GHRSST) Level-3 collated (L3C) v1.0 data were used in this study [*Le Borgne et al.,* 2006]. Only data with a 'quality_level' equal to 5 (best) were included in this analysis. The SEVIRI SSTs are calculated using a Nonlinear SST (NLSST) algorithm [*Walton et al.*, 1998] from infrared brightness temperature observations (as mentioned earlier, these were not

assimilated by the GEOS-ADAS) of the sea surface, and are a skin observation. However,during the algorithm processing the mean bias is adjusted to the nighttime buoy temperature and are therefore considered a sub-skin temperature. The sub-skin temperature corresponds to the SST directly below the skin layer [*Donlon et al.,* 2007]. SEVIRI has improved stray-light shielding and a single SST algorithm that is used for both day and night making it ideal for diurnal studies. In comparisons to in situ SST measurements over 1 year, the accuracy of the SEVIRI SSTs was estimated at -0.01K bias and 0.49 K standard deviation [*Le Borgne et al.*, 2006]. The cloud detection in the SEVIRI SSTs can miss low clouds at night, which could result in a cool bias for some night SSTs [*Derrien and Le Gléau*, 2005]. Several other studies showed that SEVIRI estimates of diurnal variability were accurate and compared well with other infrared SST retrievals [*Castro et al.*, 2014; *Gentemann et al.*, 2008; *Karagali and Høyer*, 2014]. Each file also has ECMWF Forecast 10 m wind speeds collocated with the data (now onwards referred to as SEVIRI winds).

2.3 AMSR2 SSTs

The AMSR2 instrument is carried on JAXA's Global Change Observation Mission - Water (GCOM-W) satellite, launched on May 18, 2012. Version 7.2 daily 25-km average maps of SST and wind speed are available from Remote Sensing Systems (RSS) from July 2014 through present [*Wentz et al.*, 2014]. This polar-orbiting platform results in data with an equatorial crossing time of 1:30 AM/PM (Ascending/Descending). SST data areavailable for all valid retrievals except when winds are greater than 20 $ms^{-1}$, in regions with sun glint, rain, near sea ice, or within 75 km of land. Accuracy of the AMSR2 SST retrievals has been estimated through comparisons to in situ SSTs as -0.04 K bias and 0.55 K Standard Deviation (STD) [*Gentemann and Hilburn*, 2015]. Coincident AMSR2 wind speeds are contained in the same file, also generated from the AMSR2 brightness temperatures using the RSS retrieval algorithm. Accuracy of the RSS AMSR2 wind speeds was estimated as 0.13 $ms^{-1}$ bias and 0.99 $ms^{-1}$ STD when compared to buoys [*Ebuchi*, 2014].

2.3 Calculation of diurnal warming from satellite SSTs

Calculating the diurnal warming signal present in the satellite data requires determination of the foundation SST, $T_d$ defined as the temperature free of diurnal warming [*Donlon et al.*, 2007]. This is accomplished using averages of nighttime SST values. For both SEVIRI and AMSR2 SST data, the SST data were spatially averaged onto the GEOS-5 grid and saved in daily arrays of 24, hourly, maps. Next, these data were put onto Local Mean Time (LMT) daily maps, which were used to calculate a daily $T_d$ by averaging 3 days of nighttime data from 3 AM to 6 AM LMT for SEVIRI and 1 AM to 6 AM for AMSR2. These nighttime data should represent a best-estimate of the $T_d$. The effect of this averaging will be discussed later in the document. It is possible that the nighttime average SEVIRI SST could be affected by undetected low clouds, but using multiple days should minimize the effect of any undetected clouds. Diurnal warming is then calculated as $\Delta T_{dw} = SST - T_d$.

The sensitivity (the ratio of actual over retrieved change) of the NLSST algorithm, used for determining SEVIRI SSTs was evaluated by *Merchant et al.* [2009]. The lowest sensitivity was seen in the Tropics, where there are high values of total columnar water vapor, the highest sensitivities were in higher latitudes which are normally dry compared to the Tropics. Diurnal warming studies can be affected by this water vapor content, where fluctuating SSTs in areas of high water vapor can be under-estimated by up to 33% [*Merchant et al.,* 2009]. The decrease in sensitivity is essentially due to the fact that the algorithm formulation relies on the co-variability of atmospheric and surface temperatures. When excursions from this relationship occur, such as in rapidly forming diurnal warming events, the retrieved SST will not accurately reflect changes in the actual SST. Ideally, other algorithm formulations that have a higher sensitivity, such as optimal estimation, should be used for determining IR SSTs, but these are not widely available at this point [*Merchant et al.,* 2013]. While NLSSTs may underestimate diurnal warming, they are also of a higher spatial resolution than the Passive MicroWave (PMW) SSTs. The lower spatial resolution of PMW SSTs results in an underestimation of diurnal warming as well [*Gentemann et al.*, 2008]. Both of these effects should be kept in mind when evaluating diurnal warming amplitudes determined from different satellite instruments.

## 3 Results

Diurnal warming, wind speeds, and total heat flux, $Q_{tot}$, from four days in September 2015 are shown in Figure 1. In Figure 1a, September 7, AMSR2 SSTs have the largest diurnal warming, then SEVIRI, then the GEOS-ADAS. Both SEVIRI and GEOS-ADAS wind speeds are low for the entire day, with a minimum at 12:00. The GEOS-ADAS underestimates the amount of warming, has a later peak than the satellite data, and then decreases much too rapidly after the peak, disappearing by 18:00; almost always coinciding with when the net heat flux approaches zero. The four panels show diurnal warming at different locations in the Atlantic Ocean and Mozambique Channel. All have low wind speeds during at least part of the day, leading to diurnal warming of the SSTs, however, all of them depict the evolution of the SST differently. The peak amplitude of the GEOS-ADAS warming is equal to or less than the SEVIRI satellite retrieved warming. The satellite retrieved warming shows more variability, likely due to rapidly changing winds, and also always shows more warming in the late afternoon to early evening than the GEOS-ADAS warming. Figure 1 also shows that the 25-km AMSR2 wind speed is less than or approximately equal to the GEOS-ADAS and SEVIRI wind speeds. In Figures 1a and 1c the retrieved AMSR2 wind speed is less than the GEOS-ADAS wind speed and the AMSR2 diurnal warming is larger than in GEOS-ADAS. Whereas in Figures 1b and 1d the AMSR2 wind speed is similar to the GEOS-ADAS and the warming in both of them is also of comparable amplitudes. The GEOS-ADAS warming depends heavily on the wind speeds (Equations [1] – [3]), whereas the retrievals should reflect actual warming (plus some error). Due to this important influence of the winds on the diurnal warming, we next compare the wind data.

The wind speed comparison in Figure 2 shows AMSR2 versus GEOS-ADAS and SEVIRI winds. Differences in satellite collocated wind speed and GEOS-ADAS winds will

result in differences in diurnal warming amplitude since the diurnal warming is based on the wind speeds whereas the coincident satellite winds are likely more accurate. Figure 2a shows that for winds above 3.8 $ms^{-1}$, the collocated AMSR2 winds are higher than the GEOS-ADAS winds. Figure 2b shows that the SEVIRI winds (which are operational ECMWF winds) have less bias than the GEOS-ADAS winds. Both SEVIRI and GEOS-ADAS winds are lower at low wind speeds and since diurnal warming is amplified at low wind speeds, this will affect how diurnal warming is modeled in GEOS-ADAS.

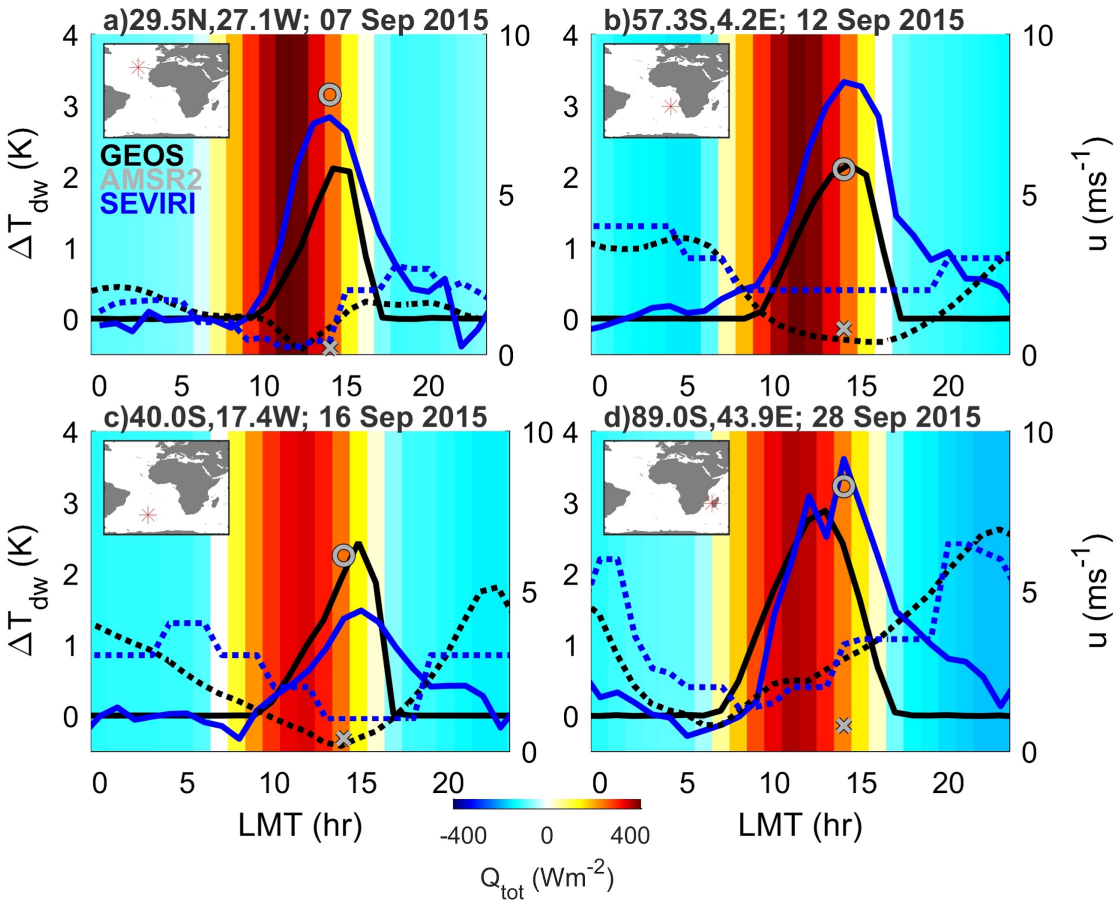


**Figure 1.** Time series of diurnal warming. SST data is shown by solid lines and 'o', with the axis on the left side of each panel. Wind speed data is shown by dashed lines and 'x', with the axis on the right side of each panel. The date and location is indicated at the top of each panel. The location of the data time series is also shown in the insert. The GEOS-ADAS data (in black) is always continuous. Days and locations were chosen partly based on availability of SEVIRI data (in blue). AMSR2 data (in gray) is only available near the local equatorial crossing time

(LECT) of 1:30 AM/PM. The background colors, $Q_{tot}$, indicate the total heat flux at the surface (latent, sensible, radiative) as calculated by GEOS-ADAS.

Next we compare the diurnal warming amplitudes by averaging the data in several different ways. The September 2015 monthly average global map of GEOS-ADAS diurnal warming at 15:00 LMT compared to collocated SEVIRI and AMSR2 data is shown in Figure 3. The satellite retrieved data (Figures 3a and 3c) show more variability than the model data (Figures 3b and 3d). The SEVIRI data (Figure 3a) collocated with the GEOS-ADAS data (Figure 3b) shows general agreement in estimated diurnal warming, with strong diurnal features in the Mozambique Channel, Mediterranean Sea, and in the mid-latitude Atlantic Ocean. Some regions, such as the South Atlantic, with little warming in the model show some warming in the SEVIRI data, likely due to errors in the satellite data and how the foundation temperature is calculated. AMSR2 diurnal warming (Figure 3c) has clear patterns in diurnal warming that are similar to GEOS-ADAS warming, but it also shows less warming in the Northern Hemisphere at high latitudes and more variability in the Southern Hemisphere. The AMSR2 warming also shows smaller amplitudes in diurnal warming than the collocated GEOS-ADAS warming (Figure 3d) in all locations except near northwestern Australia.

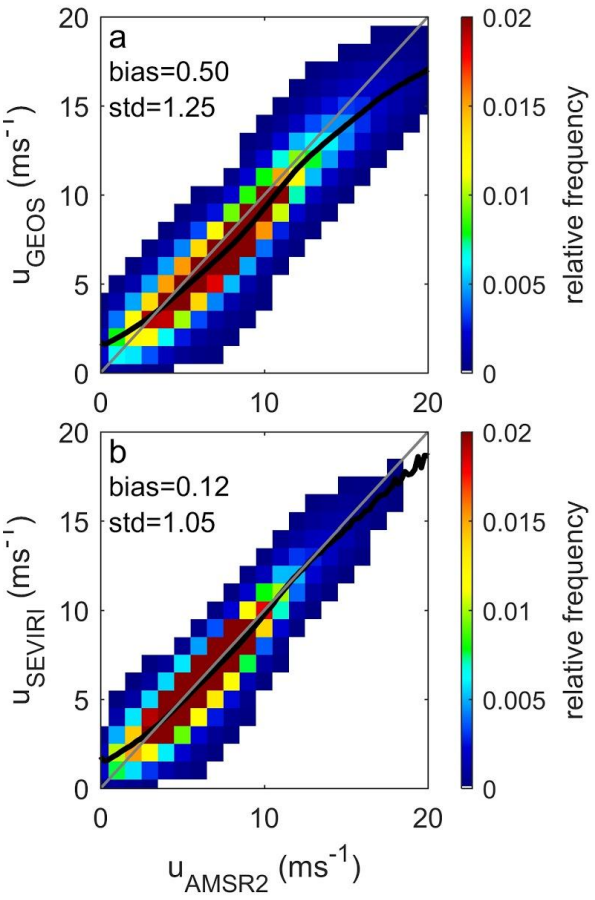


**Figure 2.** Density histogram and wind speed comparison. AMSR2 winds versus (a) GEOS-ADAS and (b) SEVIRI wind speeds. The mean is shown by the black line. A perfect fit is shown by the gray line. The bias and STD (AMSR2 minus other wind) is shown in the upper left corner. Comparisons of AMSR2 and GEOS-ADAS in panel (a) is based on global data, whereas (b) is based on data within SEVIRI field of view only.

Another way to examine the data is through a Hovmöller plot (Figure 4). Low wind systems in the Atlantic coincide with diurnal warming.. Figures 4a and 4b show SEVIRI observed and the collocated GEOS modeled warming, respectively. Figures 4c and 4d are for AMSR2 and GEOS. The SEVIRI data matches the GEOS warming more closely and with less noise, partly due to the increased number of observations available at each point from SEVIRI's hourly observations. However, to the east of Africa, GEOS-ADAS is consistently warmer than SEVIRI. Also, to the west of Africa, SEVIRI data has larger warming events (days: 240- 250 and 260- 270) than GEOS-ADAS.

Figures 5 and 6 show another analysis method by ~~is to~~ looking at the data in the same manner as *Gentemann et al.* [2003], where diurnal warming amplitudes were examined as a

function of daily average top of atmosphere (TOA) insolation ( $Q_{tot}^{av}$ ), wind speed, and LMT. Following this method, the September 2015 collocated data is shown as a function of daily average insolation, wind speed, and local mean time in Figures 5 and 6. In both comparisons, the satellite warming is less than the GEOS-ADAS warming in amplitude. Figures 5a and 5b show diurnal warming increasing linearly as a function of daily average TOA insolation. Figures 5c and 5d show an exponential decay in warming with wind speed and Figures 5e and 5f show the daily variability in warming as a function of local mean time. The most striking differences are seen in Figures 5e and 5f where the SEVIRI warming shows a slow decay in diurnal warming in the late afternoon, whereas the GEOS-ADAS warming shows a rapid decay in warming with complete disappearance by 18:00 LMT (as seen in Figure 1). Also, Figures 5c and 5d show that the GEOS-ADAS warming is larger than the SEVIRI warming at wind speeds below 2 to 3 $ms^{-1}$ (depending on daily average TOA insolation).

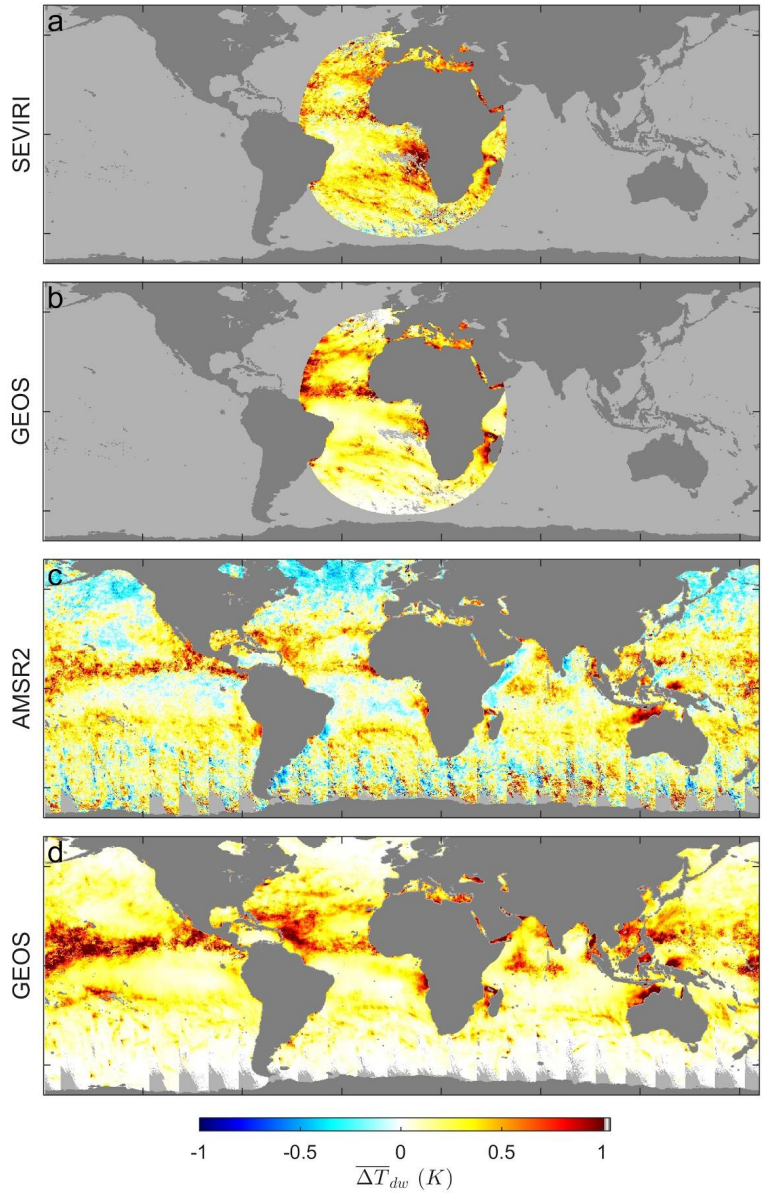


**Figure 3.** 2015 September comparison of collocated SEVIRI and AMSR2 to GEOS-ADAS diurnal warming averaged from 13:30 to 15:30 LMT. The GEOS average data in panel b(d) only includes GEOS data when valid SEVIRI(AMSR2) SSTs are available.

Figure 6 is similar to Figure 5, but shows comparisons of AMSR2 and GEOS-ADAS diurnal warming. Ideally, the foundation temperature would be calculated using only the daily

minimum temperature, which occurs at approximately 6 AM. The diurnal cycle in cloudiness has a peak at sunrise, roughly coincident with the daily minimum in diurnal heating [*Min and Zhang,* 2014]. To avoid large data gaps that would occur when the foundation temperature is 'missing' for a specific location, the nighttime data is averaged over several hours to calculate the foundation temperature. Figure 5 shows the SEVIRI estimated diurnal warming calculated as described in section 2.3. From 3 AM to 6 AM the average diurnal warming is approximately 0 K with little change from 3 AM to 6 AM. AMSR2 data (Figure 6) is from a polar-orbiter, with a LECT of 1:30 AM/PM, therefore the data used for the foundation temperature calculation is primarily centered around 1:30 AM. Since there can still be some residual warming (at low wind speeds) at this time, the SEVIRI data was used to estimate how the AMSR2 sampling would underestimate the diurnal warming. The earlier time would result in diurnal warming being underestimated by -0.04 K. This small bias can be explained as most of the nighttime data is at wind speeds where there is no diurnal warming. Only at the lowest winds will residual diurnal warming still be present this long after sunset.

Figure 6a clearly shows a problem in the satellite data at high wind speeds, with a unphysical diurnal warming values at low values of insolation. This result is somewhat expected given the distribution of `negative' warming shown in Figure 3c. When the analysis is extended for AMSR2 data over the entire year (not collocating with GEOS-ADAS data), this effect disappears, but for September 2015, AMSR2 has a `cool bias' in the Northern Hemisphere. Figure 6a shows that the diurnal warming in AMSR2 and GEOS-ADAS disappears below approximately 170 $Wm^{-2}$. Figures 6c and 6d both show an exponential decay in warming with wind speed, with very similar amplitudes in warming. Figures 6e and 6f are only able to show part of daily variability due to the AMSR2 polar orbit which has a local equatorial crossing time of 1:30 AM/PM. It is not possible to compare how the warming varies through the day with only these data points, but the largest values of warming are seen at the lowest wind speed; they are not only larger in magnitude, but have a sharper increase in warming from 14:00 to 16:00 in the GEOS-ADAS than in the AMSR2 data.

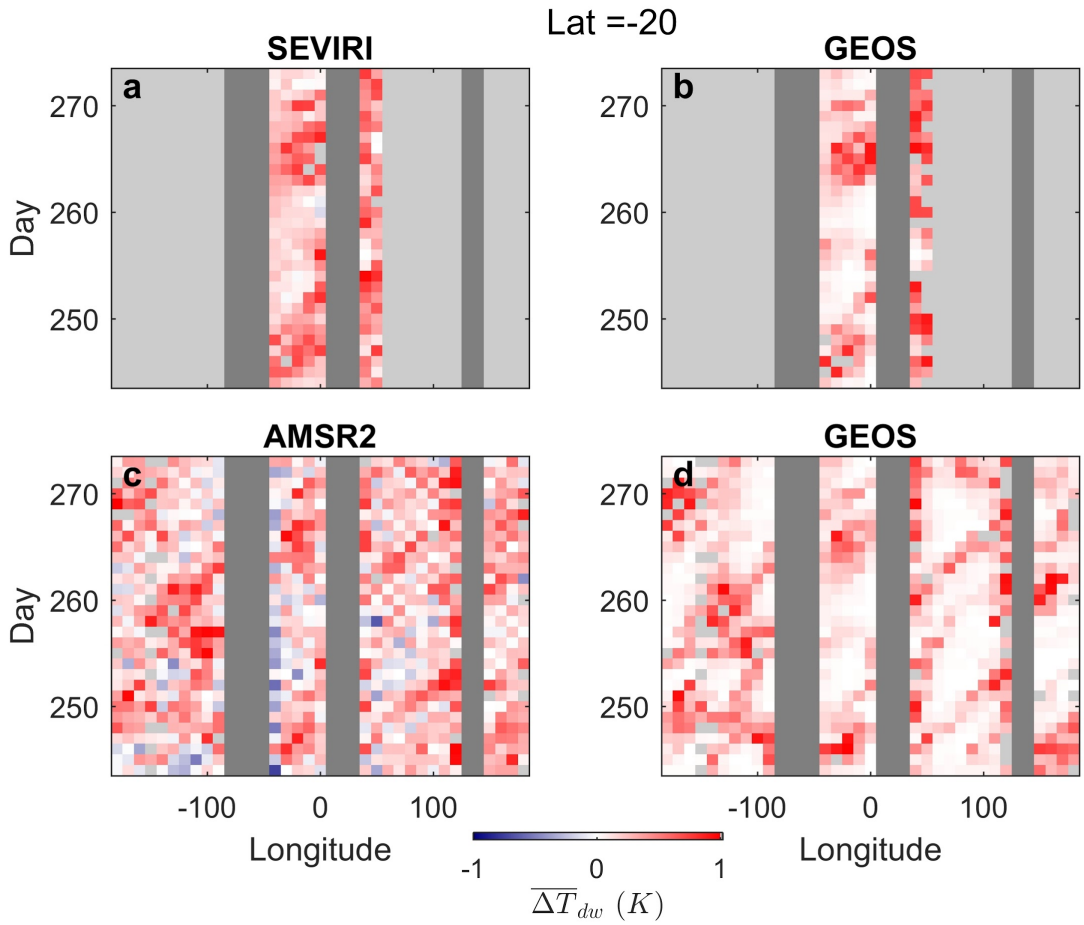


Figure 4. Hovmöller plots of the average diurnal warming, from 1PM to 3PM, at a latitude of 20 South; land (missing) points are shown in gray (light gray).

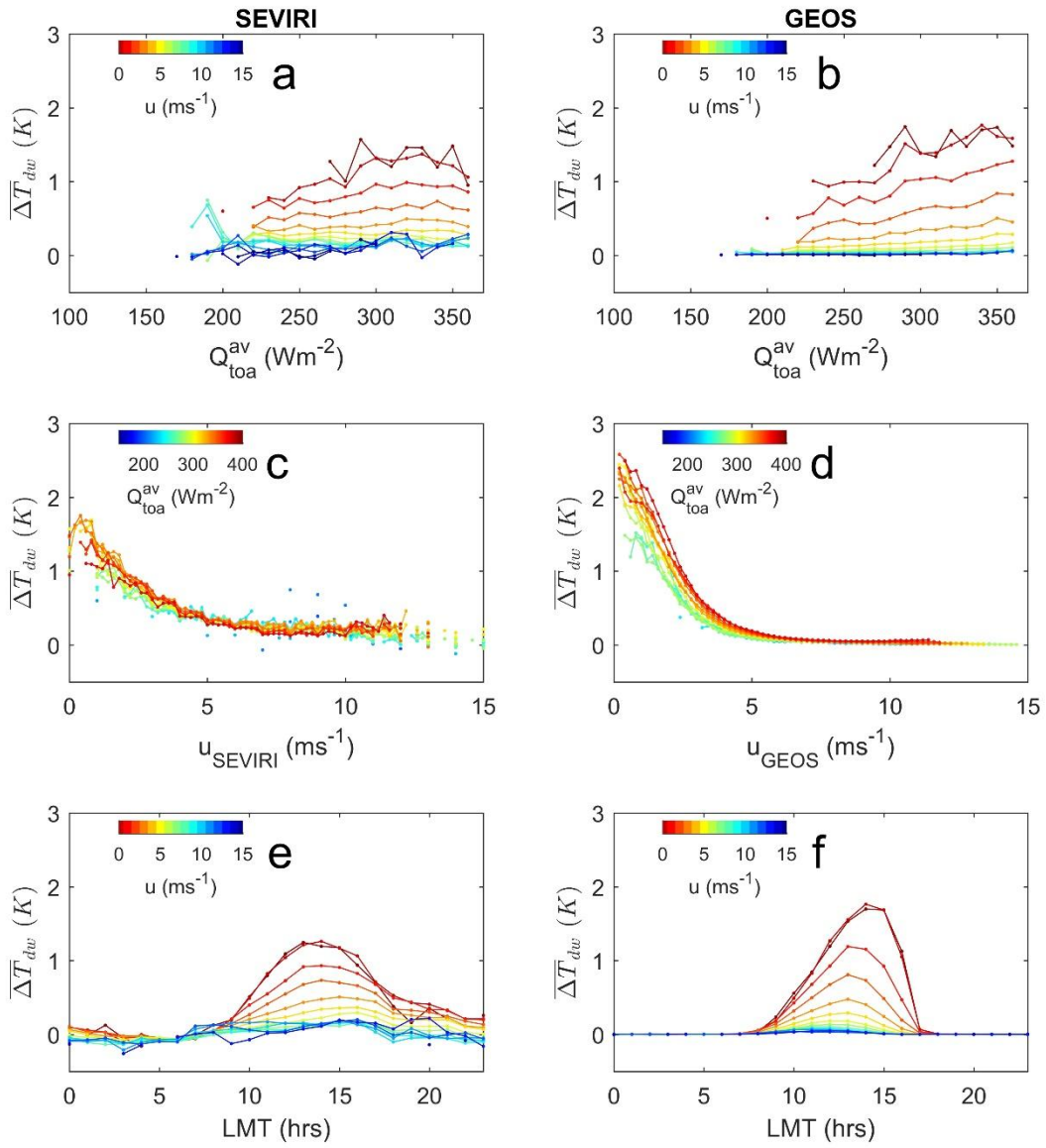


**Figure 5.** Collocated SEVIRI and GEOS-ADAS diurnal warming as a function daily average TOA insolation (a and b), wind speed (c and d), and Local Mean Time (e and f). The SEVIRI data is in the left column and the GEOS-ADAS diurnal warming in in the right column.

The dependence on wind speed on collocated diurnal warming is more clearly illustrated in Figure 7. The exponential dependence is clear in Figures 5 and 6 and to examine the decay of diurnal warming with wind speed, data were fit to following Equation [4]. Different formulations for this equation were tested and the $u^2$ in the exponent fit the data best.

$$\overline{\Delta T}_{dw}(Q_{tot}^{av}) = ae^{\frac{u2}{b}} \qquad [4]$$

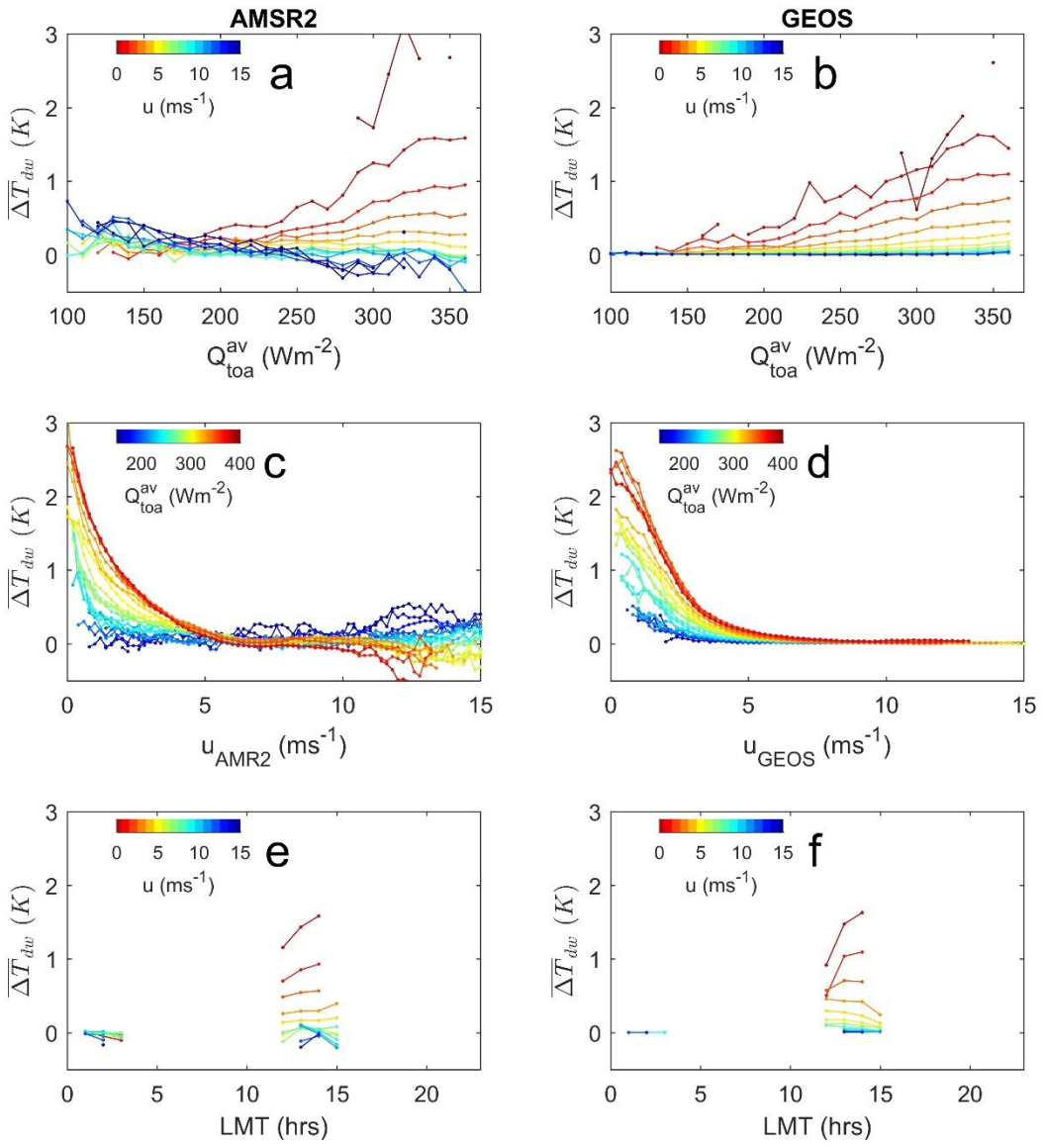


**Figure 6.** Collocated AMSR2 and GEOS-ADAS diurnal warming as a function daily average TOA insolation (a and b), wind speed (c and d), and Local Mean Time (e and f). The AMSR2 data is in the left column and the GEOS-ADAS diurnal warming in in the right column.

The coefficients *a* and *b* were determined through nonlinear least squares fit of the data shown in Figures 5 and 6. Coefficients were determined for daily average insolation values from 250 $Wm^{-2}$ to 360 $Wm^{-2}$ at a local time of 3 PM. Since the magnitude, a, is dependent on the model or data used, only the decay rate, b, is shown in Figure 7. The SEVIRI and AMSR2 wind speed decay rates are very similar, -12.7 and -13.7, respectively. The GEOS-ADAS warming for both collocations with SEVIRI and AMSR2 have the same average decay rate of -6.7. These

values yield diurnal warming less than 0.01 K above 5.6 $ms^{-1}$ for GEOS-ADAS and above 7.6 $ms^{-1}$ for the satellite observations. This results indicates that the model (Equations [1]- [3]) is not mixing heat in the upper layer in the same manner as the retrievals indicate and that the coefficients that control this in the model should be adjusted to obtain more realistic behavior to better match the observational data from satellites.

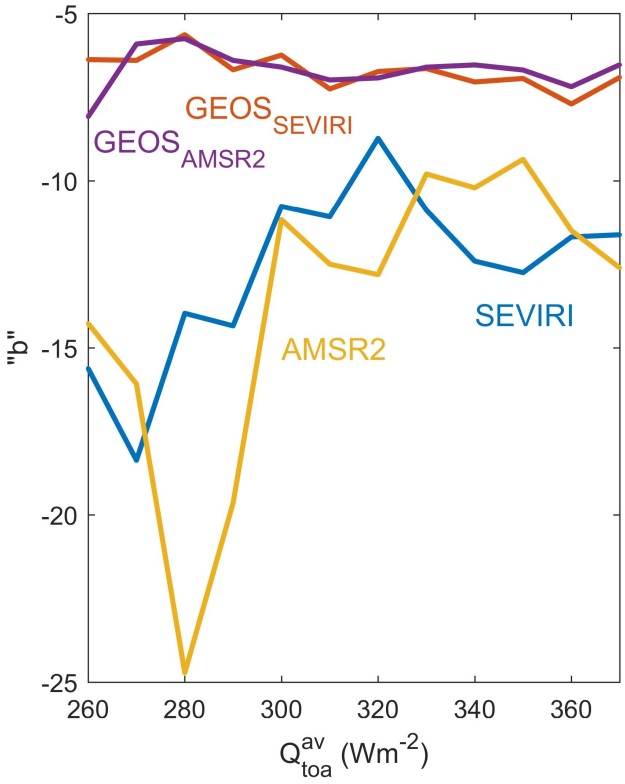


**Figure 7.** Fit to Equation 4, coefficient b and LMT equal to 15:00.

## 5 Summary and Discussions

The diurnal warming in the GEOS-ADAS model isolates the contributions of diurnal warming and cool skin effects allowing the evaluation of them separately. In the satellite observations, while the SEVIRI SSTs are determined from surface radiances, the algorithm used to calculate SSTs was developed using collocated radiance and in situ buoy SST observations. This has the effect of setting the average SEVIRI SST to a bulk temperature. The method that we use to isolate diurnal warming in the SEVIRI SSTs should remove the bulk mean difference and the resultant temperature difference will include components from cool skin effects as well as diurnal warming. For AMSR2, the retrieval is a sub-skin SST, again set to a bulk SST mean through comparisons to buoys. The temperature difference we calculate should be diurnal warming and not have much of a component from the cool skin. All the comparisons that we

have done are with the data assimilating GEOS-ADAS diurnal warming calculation, ignoring the cool skin effect. In reality this will only impact the diurnal magnitudes below 2 $ms^{-1}$, where the skin effect is largest, [*Donlon et al.,* 2002], but the difference should be negligible for the month of data that we have analyzed and we felt that this quantity was the closest to the satellite observations.

Overall the comparisons between SEVIRI, AMSR2, and GEOS-ADAS diurnal warming show encouraging results. The GEOS-ADAS warming has a realistic geographical distribution, matches satellite observed warming through the day, and roughly comparable magnitudes. Teasing out the causes for the differences in retrieved and assimilated warming is a difficult problem and requires analysis from a number of viewpoints. Amplitudes of the diurnal warming from the satellite data may underestimate the actual surface warming due to algorithm sensitivity and spatial resolution, but these effects shouldn't affect the rate of cooling/warming.

Examination of individual diurnal warming events shows the highly variable nature of diurnal warming. The GEOS-ADAS model matched AMSR2 diurnal magnitudes at 2PM local time when the model wind speeds were close to the satellite derived wind speeds. The SEVIRI warming shows the shape of warming through the day and it was more variable than the assimilated warming and also showed more warming in the late afternoon. These results were also seen in the statistical analysis of warming shown in Figures 5and 6. The GEOS-ADAS' amplitude was close to the diurnal warming seen in AMSR2, but it decayed too quickly with increasing wind speed and decreased much too rapidly in the late afternoon. The amplitude of warming depended strongly on the model wind speed. In all cases, model wind speeds collocated to satellite observations resulted in smaller amplitudes. The most accurate depiction of diurnal warming magnitudes, when looking at them in an average-sense, was when coincident satellite observations of wind speed were available for the validation (Supplemental Figure S1). The SEVIRI amplitudes are lower than GEOS-ADAS, as expected given that the NLSST algorithm sensitivity should result in an underestimation of actual amplitudes. The AMSR2 amplitudes are close to the GEOS-ADAS which should be expected given that they have similar spatial resolutions. In the future, more confidence in the diurnal warming amplitudes estimated from IR SSTs will be possible as data processed using an improved sensitivity algorithm becomes available.

Based on these comparisons, we recommend following modifications to the TBBJ10 model formulation. The Monin-Obukhov similarity model, Equation [2], changes form when the stability parameter, changes sign. In the late afternoon, the switch to heat loss causes $\zeta$ to change sign and the $\zeta < 0$ is in effect. This change results in the unrealistically rapid decay of warming (Supplemental Figure S2). The form of the similarity function in Equation [2] was developed based on *Large et al.* [1994] which discusses the dimensionless flux profiles and gives analytic expressions from available data [*Högström*, 1988]. Hence, either Equation [2] coefficients should be revisited or the implementation of TBBJ10 model in GEOS-ADAS should be revised; latter approach is being actively investigated within the GEOS- AGCM. In addition to exploring the Equation [2] coefficients, it should be recognized that the TBBJ10 model does

not parameterize any heat exchange with the bottom boundary and there is a fixed diurnal warm layer thickness, both of which are unrealistic. Heat exchanges are going to occur at both surface and bottom of diurnal warm layer through mixing and decrease the heat within the layer, and hence require coupling of the diurnal warming model with an OGCM. Also, variability in warm layer depths are well documented and should be considered in future versions of the model [*Delnore*, 1972; *Halpern and Reed*, 1976; *Soloviev and Lukas*, 1997].

**Acknowledgments, Samples, and Data**

The data from the EUMETSAT Satellite Application Facility on Ocean & Sea Ice used in this study are accessible through the SAF's homepage http://www.osi-saf.org. GHRSST SEVIRI L3C v1.0 data were downloaded from this site on 8 August 2016. AMSR2 data are produced by Remote Sensing Systems and were sponsored by the NASA AMSR-E Science Team and the NASA Earth Science MEaSUREs Program. Data are available at www.remss.com.

**References**

Akella, S., R. Todling, and M. Suarez (2017), Assimilation for skin SST in the NASA GEOS atmospheric data assimilation system, *Quarterly Journal of the Royal Meteorological Society*, *143*(703), 1032-1046, doi:10.1002/qj.2988.

Anderson, S. P., R. A. Weller, and R. B. Lukas (1996), Surface buoyancy forcing and the mixed layer of the western Pacific warm pool: Observations and 1D model results, *Journal of Climate*, *9*(12), 3056-3086, doi:10.1175/1520-0442(1996)009<3056:SBFATM>2.0.CO;2.

Bloom, S. C., L. L. Takacs, A. M. d. Silva, and D. Ledvina (1996), Data Assimilation Using Incremental Analysis Updates, *Monthly Weather Review*, *124*(6), 1256-1271, doi:10.1175/1520-0493(1996)124<1256:DAUIAU>2.0.CO;2.

Carton, J. A., and B. S. Giese (2008), A Reanalysis of Ocean Climate Using Simple Ocean Data Assimilation (SODA), *Monthly Weather Review*, *136*(8), 2999-3017, doi:0.1175/2007MWR1978.1.

Castro, S. L., G. A. Wick, and J. J. H. Buck (2014), Comparison of diurnal warming estimates from unpumped Argo data and SEVIRI satellite observations, *Remote Sensing of Environment*, *140*, 789-799, doi:http://dx.doi.org/10.1016/j.rse.2013.08.042.

Clayson, C. A., and J. A. Curry (1996), Determination of surface turbulent fluxes for the Tropical Ocean-Global Atmosphere Coupled Ocean-Atmosphere Response Experiment: Comparison of satellite retrievals and *in situ* measurements, *J. Geophys. Res.*, *101*(C12), 28515-28528, doi:10.1029/96JC02022.

Dai, A., and K. E. Trenberth (2004), The diurnal cycle and its depiction in the community climate system model, *Journal of Climate*, *17*, 930-951, doi:10.1175/1520-0442(2004)017<0930:TDCAID>2.0.CO;2.

Delnore, V. E. (1972), Diurnal variation of temperature and energy budget for the oceanic mixed layer during BOMEX, *Journal of Physical Oceanography*, *2*, 239-247, doi:10.1175/1520-0485(1972)002<0239:DVOTAE>2.0.CO;2.

Donlon, C. J., M. Martin, J. D. Stark, J. Roberts-Jones, E. Fiedler and W. Wimmer, 2011. The Operational Sea Surface Temperature and Sea Ice analysis (OSTIA). *Remote Sensing of the Environment.* doi: 10.1016/j.rse.2010.10.017 2011.

Donlon, C. J., et al. (2007), The Global Ocean Data Assimilation Experiment (GODAE) High Resolution Sea Surface Temperature Pilot Project (GHRSST-PP), *Bulletin of the American Meteorological Society*, *88*(8), 1197-1213, doi:10.1175/BAMS-88-8-1197.

Ebuchi, N. (2014), Evaluation of wind speed globally observed by AMSR2 on GCOM-W1, 2014 IEEE Geoscience and Remote Sensing Symposium, Quebec City, QC, 2014, pp. 3902-3905, doi: 10.1109/IGARSS.2014.6947337.

Fairall, C. W., E. F. Bradley, J. S. Godfrey, G. A. Wick, J. B. Edson, and G. S. Young (1996a), Cool-skin and warm-layer effects on sea surface temperature, *J. Geophys. Res.*, *101*(C1), 1295-1308, doi:10.1029/95JC03190.

Fairall, C. W., G. S. Young, E. F. Bradley, D. P. Rogers, and J. B. Edson (1996b), Bulk parameterization of air-sea fluxes for Tropical Ocean-Global Atmosphere Coupled-Ocean Atmosphere Response Experiment, *J. Geophys. Res.*, *101*(C2), 3747-3764, doi:10.1029/95JC03205.

Gentemann, C. L., C. J. Donlon, A. Stuart-Menteth, and F. J. Wentz (2003), Diurnal signals in satellite sea surface temperature measurements, *Geophys. Res. Lett.*, *30*(3), doi:10.1029/2002GL016291.

Gentemann, C. L., and K. Hilburn (2015), In situ validation of sea surface temperatures from the GCOM-W1 AMSR2 RSS calibrated brightness temperatures, *Journal of Geophysical Research: Oceans*, *120*(5), 3567-3585, doi:10.1002/2014JC010574.

Gentemann, C. L., P. J. Minnett, P. Le Borgne, and C. J. Merchant (2008), Multi-satellite measurements of large diurnal warming events, *Geophys. Res. Lett.*, *35*, doi:10.1029/2008GL035730.

Gentemann, C. L., P. J. Minnett, and B. Ward (2009), Profiles of Surface Heating (POSH): a new model of upper ocean diurnal warming, *J. Geophys. Res.*, *114*,doi:10.1029/2008JC004825.

Halpern, D., and R. Reed (1976), Heat budget of the upper ocean under light winds, *Journal of Physical Oceanography*, *6*, 972-975, doi:10.1175/1520-0485(1976)006<0972:HBOTUO>2.0.CO;2.

Högström, U. (1988), Non-dimensional wind and temperature profiles in the atmospheric surface layer: A re-evaluation, *Boundary-Layer Meteorology*, *42*(1), 55-78, doi:10.1007/bf00119875.

Karagali, I., and J. Høyer (2014), Characterisation and quantification of regional diurnal SST cycles from SEVIRI, *Ocean Science*, *10*, 745-758.

Kawai, Y., and H. Kawamura (2000), Study on a platform effect in the in situ sea surface temperature observations under weak wind and clear sky conditions using numerical models, *J. of Atmos. and Oceanic Tech*., 17, 185-197, doi:10.1175/1520-0426(2000)017<0185:SOAPEI>2.0.CO;2.

Kawai, Y., and A. Wada (2007), Diurnal sea surface temperature variation and its impact on the atmosphere and ocean: a review, *J. of Oceanography*, 63(5), 721-877, doi:10.1007/s10872-007-0063-0.

Large, W. G., J. C. McWilliams, and S. C. Doney (1994), Oceanic vertical mixing: a review and a model with a nonlocal boundary layer parameterization, *Reviews of Geophysics*, *32*(4), 363-403, doi:10.1029/94RG01872.

Le Borgne, P., G. Legendre, and A. Marsouin (2006), Operational SST retrieval from MSG/SEVIRI data, in *2006 EUMETSAT Meteorological Satellite Conference*, edited, Helsinki, Finland.

Merchant, C. J., A. R. Harris, H. Roquet, and P. Le Borgne (2009), Retrieval characteristics of non-linear sea surface temperature from the Advanced Very High Resolution Radiometer, Geophys. Res. Lett., 36(17), doi:10.1029/2009GL039843.

Merchant, C. J., P. Le Borgne, H. Roquet, and G. Legendre (2013), Extended optimal estimation techniques for sea surface temperature from the Spinning Enhanced Visible and Infra-Red Imager (SEVIRI), *Rem. Sens. of Environ*., 131, 287-297, doi:http://dx.doi.org/10.1016/j.rse.2012.12.019.

McLay, J., M. Flatau, C. Reynolds, J. Cummings, T. Hogan, and P. Flatau (2012), Inclusion of sea-surface temperature variation in the US Navy ensemble-transform global ensemble prediction system, *Journal of Geophysical Research: Atmospheres*, *117*(D19120), doi:10.1029/2011JD016937.

Min, M., and Z. Zhang (2014), On the influence of cloud fraction diurnal cycle and sub-grid cloud optical thickness variability on all-sky direct aerosol radiative forcing, *Journal of Quantitative Spectroscopy and Radiative Transfer*, 142, 25-36, doi:http://dx.doi.org/10.1016/j.jqsrt.2014.03.014.

Minnett, P. J. (2003), Radiometric measurements of the sea-surface skin temperature - the competing roles of the diurnal thermocline and the cool skin, *International Journal of Remote Sensing*, *24*(24), 5033-5047, doi:10.1080/0143116031000095880.

Price, J. F., R. A. Weller, C. M. Boewrs, and M. G. Briscoe (1987), Diurnal response of SST observed at the long term upper ocean study (34N, 70W) in the Sargasso Sea, *J. Geophys. Res.*, *92*, 14480-14490, doi:10.1029/JC092iC13p14480.

Price, J. F., R. A. Weller, and R. Pinkel (1986), Diurnal Cycling: Observations and models of the upper ocean response to diurnal heating, cooling, and wind mixing, *J. Geophys. Res.*, *91*(C7), 8411-8427, doi:10.1029/JC091iC07p08411.

Putman, W. M., and S.-J. Lin (2007), Finite-volume transport on various cubed-sphere grids, *Journal of Computational Physics*, *227*(1), 55-78, doi:http://dx.doi.org/10.1016/j.jcp.2007.07.022.

Reynolds, R. W., N. A. Rayner, T. M. Smith, D. C. Stokes, and W. Wang (2002), An improved *in situ* and satellite SST analysis for climate, *Journal of Climate*, *15*, 1609-1625, doi:10.1175/1520-0442(2002)015<1609:AIISAS>2.0.CO;2. Reynolds, R. W., T. M. Smith, C. Liu, D. B. Chelton, K. S. Casey, and M. G. Schlax (2007), Daily high-resolution blended analyses for sea surface temperature, *Journal of Climate*, *20*(22), 5473-5496, doi:10.1175/2007JCLI1824.1.

Shinoda, T., and H. H. Hendon (1998), Mixed layer modeling of intraseasonal variability in the tropical western Pacific and Indian oceans, *Journal of Climate*, *11*, 2668-2685, doi: 10.1175/1520-0442(1998)011<2668:MLMOIV>2.0.CO;2.

Soloviev, A., and R. B. Lukas (1997), Observations of large diurnal warming events in the near-surface layer of the western equatorial Pacific warm pool, *Deep-Sea Research I*, *44*(6), 1055-1076, doi:10.1016/S0967-0637(96)00124-0.

Takaya, Y., J.-R. Bidlot, A. C. M. Beljaars, and P. A. E. M. Janssen (2010a), Refinements to a prognostic scheme of skin sea surface temperature, *Journal of Geophysical Research: Oceans*, *115*(C6), doi:10.1029/2009JC005985.

Takaya, Y., F. Vitart, G. Balsamo, M. Balmaseda, M. Leutbecher, and F. Molteni (2010b), Implementation of an ocean mixed layer model in IFS, *Rep.*, ECMWF Tech Memo 622 (available from ECMWF Shinfield Park Reading RG2 9AX UNITED KINGDOM).

Vernieres, G., M. M. Rienecker, R. Kovach, and C. L. Keppenne (2012), The GEOS-iODAS:Description and Evaluation, *Rep.*, 73 pp, National Aeronautics and Space Administration, Goddard Space Flight Center, Greenbelt, Maryland.

Walton, C. C. (1988), Nonlinear multichannel algorithms for estimating sea surface temperature with AVHRR satellite data, *J. of Applied Meteo.*, 27, 115-124, doi:10.1175/1520-0450(1988)027<0115:NMAFES>2.0.CO;2.

Webster, P. J., C. A. Clayson, and J. A. Curry (1996), Clouds, radiation, and the diurnal cycle of sea surface temperature in the tropical western Pacific, *J. of Climate*, 9, 1712-1730, doi:10.1175/1520-0442(1996)009<1712:cratdc>2.0.co;2.

Wentz, F., T. Meissner, C. L. Gentemann, K. Hilburn, and J. Scott (2014), Remote Sensing Systems GCOM-W1 AMSR2 Daily Environmental Suite on 0.25 deg grid, Version 7.2. Remote Sensing Systems, Santa Rosa, CA. Available online at www.remss.com/missions/amsre. [Accessed 14 Jun 2016].

While, J., C. Mao, M. Martin, J. Roberts-Jones, P. Sykes, S. Good, and A. McLaren (2017), An operational analysis system for the global diurnal cycle of sea surface temperature: implementation and validation, *Quarterly Journal of the Royal Meteorological Society*, 143:1787-1803,, doi:10.1002/qj.3036.

Yokoyama, R., S. Tanba, and T. Souma (1995), Sea surface effects on the sea surface temperature estimation by remote sensing, *International Journal of Remote Sensing*, *16*, 227-238, doi: 10.1080/01431169508954392.

Zeng, X., and A. Beljaars (2005), A prognostic scheme of sea surface skin temperature for modeling and data assimilation, *Geophys. Res. Lett.*, *32*, doi:10.1029/2005GL023030.

Zeng, X., and R. E. Dickinson (1998), Impact of diurnally-varying skin temperature on surface fluxes over the tropical Pacific, *Geophys. Res. Lett.*, *25*(9), 1411-1414, doi:10.1029/98GL51097.